ELSEVIER

Journal of Chromatography A, 771 (1997) 9–22

JOURNAL OF CHROMATOGRAPHY A

Productivity and operating regimes in protein chromatography using low-molecular-mass displacers

Stuart R. Gallant, Steven M. Cramer*

Howard P. Isermann Department Chemical Engineering, Rensselaer Polytechnic Institute, Troy, NY 12180, USA

Received 24 September 1996; revised 18 November 1996; accepted 18 November 1996

Abstract

A theoretical and experimental study of ion-exchange displacement chromatography using the low-molecular-mass displacer neomycin sulfate, is carried out. A chromatography model utilizing the steric mass action (SMA) ion-exchange formalism is employed to predict the displacement behavior of proteins displaced by neomycin sulfate. An operating regime plot is developed from the SMA model to predict selective displacement chromatography using low-molecular-mass displacers. Numerical simulations are employed to examine the behavior of selective displacement systems and to investigate the productivity of displacement chromatography. In this study, it is seen that use of low-molecular-mass displacers allows "selective displacement" separations in which some impurities are removed by elution or by desorption within the displacer front. Further, low-molecular-mass displacers, like previously studied high-molecular-mass displacers, can provide high productivity chromatographic separations even for feed streams characterized by low separation factors.

Keywords: Preparative chromatography; Displacement chromatography; Steric mass action model; Displacers; Proteins; Neomycin sulfate; Cytochrome *c*; Lysozyme

1. Introduction

Displacement chromatography is one of the four operating modes of preparative chromatography [1–3], the other three being isocratic, step gradient and continuous gradient chromatography. In displacement chromatography, a large mass of a feed solution containing one or several product molecules is loaded onto the chromatography column and immediately followed with a displacer front. The displacer drives the feed components forward through the column and causes a separation based on chromatographic affinity. The purified components form square isotactic bands which are recovered during faction collection.

Displacement chromatography was first modelled within a constant separation factor framework [4–7]. Using the "h-transform" or "Ω-transform," these authors were able to develop relatively simple models describing ideal displacement development in constant separation factor systems. A number of authors have extended and expanded this work on displacement to consider a variety of experimental systems, to address issues of finite rates of mass transfer, and to examine the optimum operating conditions for displacement chromatography using the Langmuir or monovalent ion-exchange isotherms [8–15] or the modifier dependent Langmuir isotherm [16,17]. Since constant separation factor isotherms

*Corresponding author.

PII S0021-9673(96)01042-4

do not explain all of the experimental results reported in the literature, researchers have begun to turn to other adsorption formalisms [18–26]. In ion-exchange chromatography of proteins, the steric mass action (SMA) model has made it possible to represent multicomponent competitive protein adsorption over a range of salt concentrations [23,27]. Since its introduction, the SMA isotherm has been used to explain a wide variety of experimental ion-exchange observations in displacement chromatography [28–37] and in elution chromatography [27,38,39].

In the work described below, the SMA formalism will be employed to study the displacement behavior of the antibiotic neomycin sulfate, one of a much larger class of molecules known as "low-molecular-mass" displacers [33,35–37]. In ion-exchange displacement chromatography, low-molecular-mass displacers have the unique ability to displace (remove proteins from the stationary phase by creating an isotactic displacement train), desorb (remove proteins from the stationary phase by the mass action of the displacer occurring within the displacer zone), or elute (remove proteins from the stationary phase by the mass action of the mobile phase salt occurring within the induced salt gradient) [37]. This phenomena, which was predicted by SMA theory, is known as "selective displacement." In contrast, Langmuirian theory requires that different displacers (having a range of affinities) must be employed in order to gain the same degree of control of the displacement process offered by SMA theory [9]. This inability of Langmuirian theory to adequately predict experimental results in protein displacement chromatography is due to the fact that the multicomponent Langmuir isotherm requires identical characteristic charge of all compounds present in the mobile phase [40]. Thus, as noted by other authors [41], the validity of previous studies of the optimization of displacement chromatography based on the multicomponent Langmuir isotherm is limited to relatively small molecules with little variation of characteristic charge. In contradistinction, SMA theory has the ability to model the adsorption of molecules ranging from low characteristic charge (salts and low-molecular-mass displacers) to intermediate and high characteristic charge (proteins and large polyelectrolytes).

In the first part of this study, the displacement separation of the proteins cytochrome *c* and lysozyme will be carried out experimentally and simulated mathematically using the SMA formalism. Subsequently, the model will be used to simulate a range of complex multicomponent displacement behavior and to explore the productivity of separations using the displacer neomycin sulfate. Finally, the advantages of being able to conduct "selective displacement" separations which include elution, displacement and desorption are discussed.

2. Theory

2.1. Equilibrium formalism

The SMA formalism is a three parameter model of ion-exchange designed specifically for representation of multicomponent protein–salt equilibrium in ion-exchange chromatography [23]. The protein is bound to the stationary phase at a number of exchange sites given by its characteristic charge, ν_i. In addition, binding of the protein sterically shields or blocks a number of sites given by its steric factor, σ_i. Finally, the equilibrium of the exchange process is represented by an equilibrium constant, K_{1i}.

The equilibrium constant of the reaction may be written:

$$K_{1i} = \left(\frac{Q_i}{C_i}\right)\left(\frac{C_1}{Q_1}\right)^{\nu_i} \quad i = 2, \ldots, \mathrm{NC} \tag{1}$$

where C_i and Q_i refer to the concentration of protein in the mobile phase and on the stationary phase, C_1 refers to the concentration of salt in the mobile phase and Q_1 refers to the concentration of bound salt available for exchange.

Each protein molecule may sterically shield some salt counterions on the adsorptive surface. The quantity of salt counterions blocked by a particular protein will be proportional to the concentration of that protein on the surface:

$$\hat{Q}_{1i} = \sigma_i Q_i \quad i = 2, \ldots, \mathrm{NC} \tag{2}$$

Electroneutrality requires that:

$$\Lambda = \bar{Q} c_1 + \sum_{i=2}^{\mathrm{NC}} (\nu_i + \sigma_i) Q_i \tag{3}$$

2.2. Operating regime plot

As mentioned in the Section 1, low-molecular-mass displacers employed in ion-exchange chromatography have the unique ability to perform "selective displacement." In selective displacement, it is possible that any given component of the feed stream will be eluted in the induced salt gradient, displaced, or desorbed in the displacer front. In order to depict the operating regimes of selective displacement chromatography, an operating regime plot has been developed.

Brooks and Cramer have shown that the boundary between two components of an isotactic displacement train will be stable when [29]:

$$\frac{K_{1A}^{\nu_B}}{K_{1B}^{\nu_A}} < \delta^{(\nu_B - \nu_A)} \tag{4}$$

where A is the displaced component and B is the displacer, K_{1i} is the equilibrium constant, ν_i is the characteristic charge and δ is the partition coefficient of the displacer (its stationary phase concentration divided by its mobile phase concentration). The "critical displacer partition ratio" is the value of δ for which Eq. (4) is satisfied. Rearranging Eq. (4), the critical displacer partition ratio with respect to a particular protein is:

$$\delta_{CD} < \frac{K_{1P}^{\nu_D/(\nu_D - \nu_P)}}{K_{1D}^{\nu_P/(\nu_D - \nu_P)}} \tag{5}$$

where the subscripts D and P refers to the displacer and the protein, respectively. Not all displacers have a critical displacer concentration. In particular, SMA theory predicts that a displacer which has a larger characteristic charge and a larger equilibrium constant than a given protein will always be able to displace that protein regardless of the displace and salt concentrations. However, a low-molecular-mass displacer will generally have a critical partition ratio at which it ceases to act as a displacer and begins to act as a desorbent [37]. The concept of a critical displacer partition ratio is valuable because it represents all of the possible combinations of displacer concentration and carrier salt concentration at which the displacer ceases to be effective.

The critical salt concentration corresponding to an arbitrary value of C_D is given by:

$$C_{1,CD} = \left(\frac{K_{1D}}{\delta_{CD}}\right)^{1/\nu_D} (\Lambda - ((\nu_D + \sigma_D) C_D \delta_{CD})) \tag{6}$$

where Λ is the bed capacity and ν_D and σ_D are the displacer characteristic charge and steric factor. By selecting values of C_D and substituting them into Eq. (6), the boundary between displacement and desorption may be mapped onto a plot of salt concentration versus displacer concentration. In Fig. 1, the boundary between displacement and desorption is shown as a solid line. To the left of the line, desorption occurs; to the right, displacement occurs.

If the induced salt gradient is too large, a protein may be eluted from the column rather than being displaced. If the protein elutes, its partition ratio in the induced gradient will be less than the partition ratio of the displacer:

$$K_{1P} \left(\frac{\Lambda}{C_{1,f} + \nu_D C_D}\right)^{\nu_P} < \delta \tag{7}$$

where $C_{1,f} + \nu_D C_D$ is the total concentration of salt that the protein experiences (carrier salt concentration plus induced gradient). At the boundary between displacement and elution, the protein's partition ratio in the induced gradient will equal that of the displacer

$$K_{1P} \left(\frac{\Lambda}{C_{1,f} + \nu_D C_D}\right)^{\nu_P} = \delta. \tag{8}$$

Recall that the partition ratio of the displacer is given by the following expression (the SMA single component isotherm):

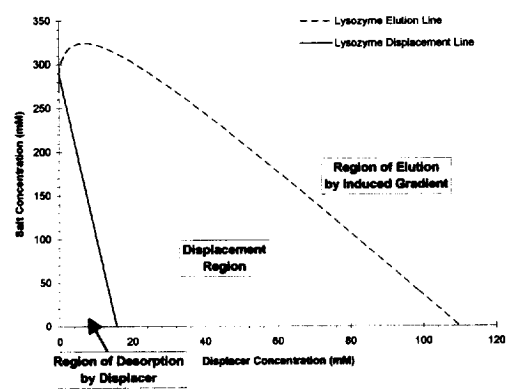

Fig. 1. Operating regime plot.

$$\delta = K_{1D}\left(\frac{\Lambda - ((\nu_D + \sigma_D)Q_D}{C_{1,f}}\right)^{\nu_D}. \quad (9)$$

Combining the two preceding equations and eliminating $C_{1,f}$, an analytical expression can be written for the critical displacer concentration at which elution of the protein in the induced gradient occurs:

$$C_{D,CE} = \frac{\Lambda\left(1-\left(\frac{K_{1D}}{\delta}\right)^{1/\nu_D}\left(\frac{\delta}{K_{1P}}\right)^{1/\nu_P}\right)}{\left(\frac{\delta}{K_{1P}}\right)^{1/\nu_P}\left(\nu_D - \left(\left(\frac{K_{1D}}{\delta}\right)^{1/\nu_D}(\nu_D + \sigma_D)\delta\right)\right)}. \quad (10)$$

The corresponding critical salt concentration at elution can be conveniently calculated:

$$C_{1,CE} = \left(\frac{K_{1D}}{\delta}\right)^{1/\nu_D}(\Lambda - ((\nu_D + \sigma_D)C_{D,CE}\delta)). \quad (11)$$

By selecting values of the displacer partition coefficient δ and substituting them into Eq. (10) and Eq. (11), the boundary between displacement and elution may also be mapped onto a plot of salt concentration versus displacer concentration. In Fig. 1, the boundary between displacement and elution is shown as a dashed line. To the left of the line, displacement occurs; to the right, desorption occurs.

A plot of salt concentration versus displacer concentration which includes the transition boundary between displacement and desorption and the transition boundary between elution and displacement is called an operating regime plot. Such a plot is by definition specific to a particular protein and a particular displacer. However, by overlaying several plots for a particular displacer paired with each of the major components in a feed mixture to be purified, it is possible to gain significant insight into the effect of displacer concentration and salt concentration on a given separation. This technique will be employed below within the results and discussion.

2.3. Chromatographic model

The model of chromatography employed in this work employed the SMA formalism along with a single parameter, lumped dispersion model of mass transport [34,38,39]. In order to solve the system of partial differential equations which constituted the chromatographic model, a numerical technique developed by Guiochon and coworkers was employed [42,43]. In this finite difference method, a simple relation exists between the observed efficiency of the chromatography column, the effective dispersion coefficient of the transport equation and the dimensions of the finite difference grid:

$$\frac{H}{L} = \frac{2D_i}{Lu_0} = \Delta z - \frac{1}{1+k'}\Delta\tau \quad (12)$$

where H is the height equivalent to a theoretical plate, L is the column length and k' is the capacity factor in linear chromatography. Using the model, simulated chromatograms of displacement chromatography were generated [38,44]. The program was run on an IBM ES/9000 Model 580 mainframe computer using IBM VS FORTRAN under the MTS operating system.

2.4. Chromatographic productivity

The production rate of a process can be defined using the equation:

$$PR_i = \frac{C_{i,f}V_fY_i}{t_{cyc}V_{sp}} \quad (13)$$

where $C_{i,f}$ is the feed concentration of the ith component, V_f is the feed volume, Y_i is the yield, t_{cyc} is the cycle time and V_{sp} is the stationary phase volume. The numerator represents the mass of protein purified in a single cycle. The denominator represents the time and the amount of stationary phase required to produce that mass of protein. Maximization of the production rate will allow the largest quantity of purified product to be produced in the shortest amount of time with the least amount of stationary phase.

In order to calculate the production rate PR_i, the yield Y_i must be calculated:

$$Y_i = \frac{\int_{\tau_1}^{\tau_2} C_i d\tau}{C_{i,f}\tau_f} \quad (14)$$

where the cut times τ_1 and τ_2 are selected to maximize the yield at the specified purity.

The cycle time is defined as:

$$t_{cyc} = t_0(\tau_f + \tau_{sep} + \tau_{regen}) \quad (15)$$

where τ_f is the nondimensional feed time, τ_{sep} is the nondimensional separation time, τ_{regen} is the time required to regenerate and re-equilibrate the column and t_0 is the transit time of an unretained component through the column. τ_{sep} is calculated from the end of the feed injection until the breakthrough of the displacer. τ_{regen} is taken as 7.0, a value typical of the time required to remove high affinity components from a chromatography column and subsequently re-equilibrate the column.

3. Experimental

3.1. Materials

Sodium monobasic phosphate, sodium dibasic phosphate, *N*-α-benzoyl-L-arginine ethyl ester (BAEE), neomycin sulfate, horse heart cytochrome *c* and chicken egg lysozyme were purchased from Sigma (St. Louis, MO, USA). Sodium chloride was purchased from Aldrich (Milwaukee, WI, USA). Phosphoric acid was purchased from Fisher Scientific (Rochester, NY, USA). The 15 μm Source 15S strong cation exchange resin employed in this work was a gift from Pharmacia Biotech (Lilistrom, Norway). The stationary phase was packed into two Pharmacia glass columns (53.5×5 mm I.D. and 101×5 mm I.D.). The shorter column was employed during parameter estimation and fraction analysis. The longer column was employed during displacement experiments.

3.2. Apparatus

The chromatograph employed in this work consisted of two Model P-500 pumps (Pharmacia LKB, Uppsala, Sweden) connected to the chromatographic column via a Valco 10-port manual valve (Valco, Houston, TX, USA). During parameter estimation, the column effluent was monitored using a Model 757 Spectroflow UV–Vis absorbance detector (Applied Biosystems, Foster City, CA, USA) and a Powermate 2 personal computer (NEC, Tokyo, Japan) running Maxima 820 data collection software (Waters Chromatography Division, Millipore). During displacement experiments fractions of the column effluent were collected directly from the column using a Model 2212 Helirac fraction collector (Pharmacia LKB). During fraction analysis, a Spectroflow 757 UV–Vis absorbance detector (Applied Biosystems) was employed to monitor the column effluent, and a Model C-R3A Chromatopac integrator (Shimadzu, Kyoto, Japan) was employed for data acquisition and analysis.

3.3. Procedures

3.3.1. SMA parameters of proteins

The SMA parameters of the proteins cytochrome *c* and lysozyme appear in Table 1. The estimation of protein adsorption parameters has been discussed previously [27,44]. In order to estimate the characteristic charge ν_i and equilibrium constant K_{1i} of the protein, linear elution experiments were conducted over a range of mobile phase salt concentrations. The resulting data was fitted to the following linearized equation:

$$\log(k_i') = \log(\beta K_{1i} \Lambda^{\nu_i}) - \nu_i \log(C_1) \quad (16)$$

This fitting procedure provided the estimates of the characteristic charge ν_i and equilibrium constants K_{1i} of the protein.

In order to estimate the steric factors σ_i, nonlinear frontal experiments were carried out over a range of mobile phase salt and protein concentrations.

$$C_{2,SMA} = \left(\frac{C_{1,f}}{\Lambda - (\nu_i + \sigma_i)Q_{2,f}}\right)^{\nu_i} \frac{Q_{2,f}}{K_{1i}} \quad (17)$$

This equation was used in conjunction with the experimental protein isotherms in order to estimate the steric factors σ_i. The residuals between the experimental protein concentration ($C_{2,f}$) and the estimated protein concentration ($C_{2,SMA}$) were calculated as a function of the steric factor. Minimization of the sum of squares of the residuals using a Newton–Raphson technique established the estimated steric factors given in Table 1.

The displacement experiments were carried out at

Table 1
Parameters employed in simulations

Column dimensions:	101×5 mm I.D.
Column capacity (Λ):	400 mM
Void fraction (ϵ):	0.67
Flow rate:	0.25 ml/min
Effective dispersion coefficient (D_i):	5.4×10^{-4} cm^2/s
Number of theoretical plates (N):	300

Component	Characteristic charge (ν_i)	Steric factor (σ_i)	Equilibrium constant (K_{1i})
Counter ion			
Sodium ion	1.0	0.0	1.0
Proteins			
Cytochrome c	6.0	28	1.2×10^{-1}
Lysozyme	5.5	14	1.1
Artificial component 1	6.0	28	5.9×10^{-2}
Artificial component 2	5.4	15	2.5×10^{-2}
Artificial component 3	6.0	28	2.1×10^{-1}
Displacer			
Neomycin sulfate	3.8	0.0	2.0

0.25 ml/min. In order to estimate the effective dispersion coefficient to be employed in Eq. (12), the number of theoretical plates (N) and the corresponding plate height (H) were determined by measuring the width at half-height of separate dilute injections of cytochrome c and lysozyme. An average of the resulting lumped dispersion coefficients, 5.4×10^{-4} cm^2/s, was employed in the simulations.

3.3.2. SMA parameters of neomycin sulfate

The SMA parameters of the neomycin sulfate appear in Table 1. The estimation of displacer adsorption parameters has been discussed previously [44]. The characteristic charge ν_i was estimated from the induced salt gradient produced during frontal experiments:

$$\nu_i = \frac{C_{1,\mathrm{ind}}}{C_{\mathrm{D}}} \tag{18}$$

where C_{D} is the displaced concentration during the frontal experiment and $C_{1,\mathrm{ind}}$ is the magnitude of the induced salt gradient.

In order to estimate the steric factor σ_i and the equilibrium constant K_{1i}, Eq. (17) was used in conjunction with the experimental displacer isotherm. The residuals between the experimental protein concentration ($C_{2,\mathrm{f}}$) and the estimated protein concentration ($C_{2,\mathrm{SMA}}$) were calculated as a function of the equilibrium constant and steric factor. Minimization of the sum of squares of the residuals using a Newton–Raphson technique established the estimates given in Table 1.

3.3.3. Displacement chromatography

Displacement chromatography carried out at room temperature at a flow rate of 0.25 ml/min using a carrier buffered with sodium phosphate, pH 6.0; the caption gives specific experimental conditions. The feed solution was prepared by dissolving cytochrome c and lysozyme in the carrier. The displacer was prepared by dissolving neomycin sulfate in the carrier. Prior to the beginning of each displacement, the strong cation-exchange column (101×5 mm I.D.) was equilibrated with the carrier. Subsequently, the feed solution was loaded into the column and followed immediately by the displacer. Fractions (150 μl) of the column effluent were collected for subsequent analysis.

3.3.4. Protein analysis

Analysis of the collected fractions for their protein

concentration was carried out by ion-exchange chromatography using a strong cation-exchange column (53.5×5 mm I.D.) under isocratic conditions at a flow rate of 1.0 ml/min. Fractions were diluted 10–100 fold with deionized water, and 20 μl samples were injected. A mobile phase of 30 m*M* sodium phosphate and 185 m*M* sodium chloride, pH 6.0, was employed for analysis of the cytochrome *c*. Lysozyme analysis was conducted using a mobile phase of 30 m*M* sodium phosphate and 240 m*M* sodium chloride, pH 6.0. The column effluent was monitored at 280 nm. The compositional data from the protein analysis was used to generate a histogram representing the displacement experiment.

4. Results and discussion

This study considers the use of the low-molecular-mass displacer neomycin sulfate. Its application to displacement chromatography was originally reported by Kundu et al. [36]. In this study, a mathematical model is used to explore the displacement behavior of neomycin sulfate. Of particular interest is the ability of low-molecular-mass displacers to provide selective displacement [37]. An operating regime plot for convenient depiction and understanding of the experimental conditions which lead to elution, displacement, or desorption was developed in Section 2 of this paper and will be employed below.

The SMA adsorption parameters of neomycin sulfate and the proteins employed in this study, listed in Table 1, were determined using the procedures described in Section 3.3. These parameters were employed to simulate a displacement of the proteins cytochrome *c* and lysozyme. The simulated conditions included a feed injection of 6.9 dimensionless time units (9 ml) containing 0.2 m*M* (2.5 mg/ml) cytochrome *c* and 0.2 m*M* (2.9 mg/ml) lysozyme in a carrier which contained 50 m*M* sodium ion concentration and a displacer concentration of 20 m*M* neomycin sulfate in the same carrier. In Fig. 2a, the simulated displacement chromatogram of cytochrome *c* (dashed line), lysozyme (solid line) and neomycin sulfate is presented. As seen in the figure, cytochrome *c* forms a square isotactic zone while the lysozyme band displays a slight forward arc. This arc

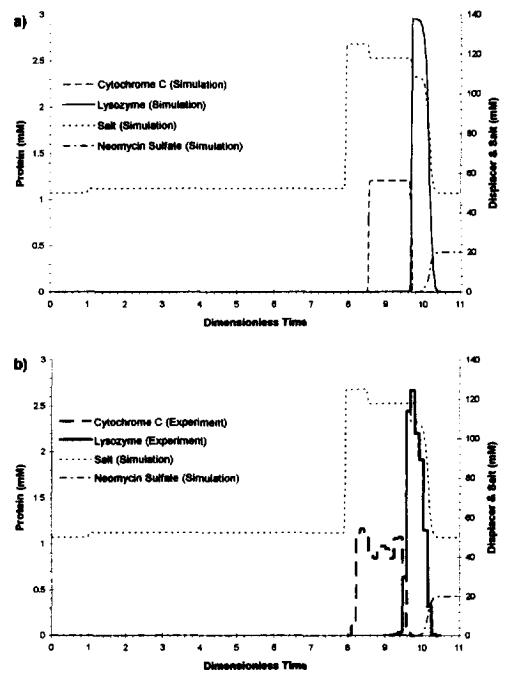

Fig. 2. Comparison of simulated and experimental displacement chromatograms. (a) Experimental displacement chromatogram. Feed Injection: 6.9 dimensionless time units of 0.2 m*M* cytochrome *c* and 0.2 m*M* lysozyme in 50 m*M* sodium ion concentration carrier (20 m*M* from NaCl and 30 m*M* from sodium phosphate). Displacer: 20 m*M* neomycin sulfate in 50 m*M* sodium ion concentration carrier. Operating Conditions: 0.25 ml/min, pH 6.0, 150 μl fractions. (b) Simulated chromatogram.

can be attributed to the high affinity of lysozyme for the stationary phase. At 20 m*M* concentration, neomycin sulfate is close to the minimum displacer concentration required to displace lysozyme at this carrier salt concentration. (With a carrier containing 50 m*M* sodium ion concentration, the minimum concentration of displacer required for displacement of lysozyme is about 13 m*M*, as seen in Fig. 1.)

Subsequently, an experiment was carried out under the same operating conditions described for Fig. 2a. Fig. 2b depicts the histograms of cytochrome *c* (dark dashed line) and lysozyme (dark solid line) obtained experimentally from analysis of the fractions. In the experiment as in the simulation, cytochrome *c* forms a wide square isotactic peak, and lysozyme's band displays a slight forward arc. The overlap between the chromatographic bands is minimal showing that an effective displacement was

achieved using the low-molecular-mass displacer neomycin sulfate.

4.1. Productivity of displacement using small displacers

Based on the good agreement of theory and experiment seen above and on previous work modelling nonlinear chromatography [27,32,34,38], it was concluded that this chromatographic model constituted a good tool for exploring the productivity of preparative displacement separations. Having tested the model on a relatively simple two-component separation, numerical simulation was subsequently employed to explore more difficult separation problems characterized by lower separation factors.

Two model separation problems were chosen as prototypical of challenges that are encountered in downstream processing. Fig. 3 shows the log(capacity factor) versus log(salt concentration) plots of components present in these problems. In both problems, cytochrome *c* was taken to be the product, and its production rate was calculated using Eq. (14). In the first problem, lysozyme was taken to be a relatively easy to separate higher affinity impurity, and artificial component 1 (dotted line) was taken to be a more difficult to separate lower affinity impurity. In the second problem, artificial component 2 (dashed line) was taken to be a relatively easy to separate lower affinity impurity, and artificial component 3 (dash-dotted line with open circle) was taken to be a more difficult to separate higher affinity impurity.

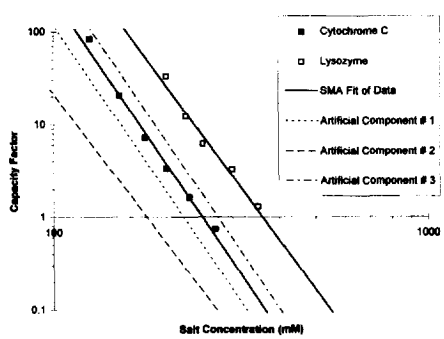

Fig. 3. Log(capacity factor) versus log(salt concentration) plot for model feed mixtures. Experimental data on the retention of horse heart cytochrome *c* (■) and lysozyme (□) on Pharmacia Source 15S strong cation exchanger. SMA representations (solid lines) of the capacity factors of cytochrome *c* and lysozyme. Artificial components 1 (dotted line) and 3 (dash–dotted line) have SMA adsorption parameters close to those of cytochrome *c*. Artificial component 2 (dashed line) is substantially less retained than cytochrome *c*.

4.2. Separation problem 1 by displacement

The problem of optimization of ion-exchange displacement chromatography on a given column has three dimensions: carrier salt concentration, displacer concentration and feed injection size. The first dimension has been investigated by Gadam et al. who showed that ion-exchange displacement separations are most productive under low carrier salt conditions [34]. However, there is a practical lower limit on carrier salt concentration. Below this salt concentration, dispersion between the chromatographic bands (due to slow desorption kinetics) increases and leads to loss of yield. Because the zones achieved in the experimental separation of cytochrome *c* and lysozyme where sharp and characterized by little overlap at 50 m*M*, this salt concentration was selected to be the carrier salt for the simulations. The remaining two variables, displacer concentration and feed injection size, interact. To study their interaction, a parametric study was carried out.

Again, the first model separation problem that was examined was a separation of cytochrome *c* (the product) from a less retained impurity (artificial component 1) and a more strongly retained impurity (lysozyme). Fig. 4 presents an operating regime plot for this problem. In the figure, the dashed line with open squares represents the elution transition line of lysozyme, and the solid line with filled squares represents the desorption transition line of lysozyme. The elution lines of the other two proteins depicted in Fig. 4a (dashed line with open triangles and dashed line with open circles) have a similar shape to that of lysozyme. Because these proteins have lower affinity for the stationary phase than lysozyme, their lines fall below lysozyme's elution line indicating that these two proteins elute at lower carrier salt concentrations. The displacement lines of the other two proteins depicted in Fig. 4b (solid line with filled triangles and solid line with filled circles) fall extremely close to the salt concentration axis. This

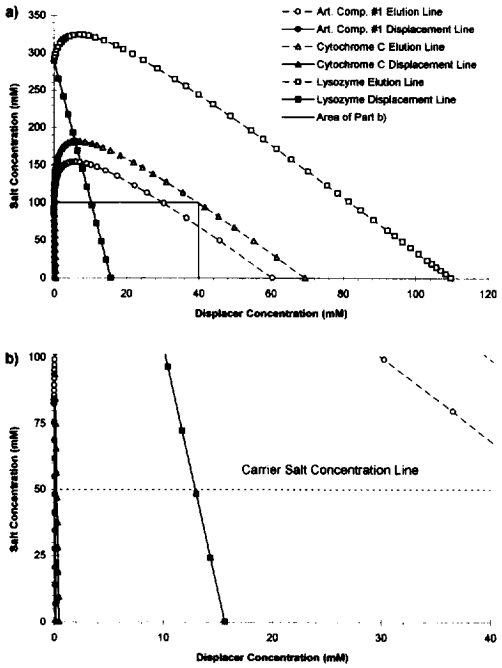

Fig. 4. Operating regime plot of feed stream 1. Elution and displacement lines of lysozyme (squares), cytochrome *c* (triangles), and artificial component 1 (circles) displaced by neomycin sulfate on strong cation exchanger. (a) Expanded view. (b) Close-up view.

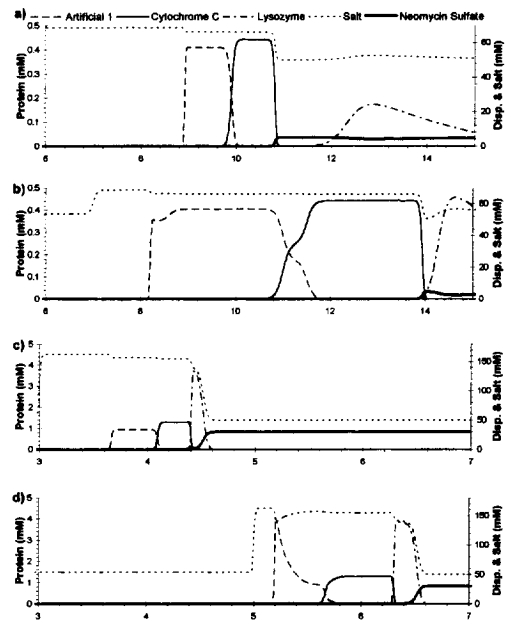

Fig. 5. Simulated displacement separations of feed stream 1. Displacement of 0.2 m*M* artificial component 1, 0.2 m*M* cytochrome *c* and 0.2 m*M* lysozyme by neomycin sulfate in 50 m*M* sodium ion concentration carrier. (a) 2.0 dimensionless time unit feed; 5 m*M* neomycin sulfate. (b) 6.0 dimensionless time unit feed; 5 m*M* neomycin sulfate. (c) 2.0 dimensionless time unit feed; 30 m*M* neomycin sulfate. (d) 4.0 dimensionless time unit feed; 30 m*M* neomycin sulfate.

indicates that almost any concentration of neomycin sulfate should be capable of displacing these proteins regardless of carrier salt concentration. Over the displacer concentration range from 0 to 40 m*M* neomycin sulfate with a carrier sodium ion concentration of 50 m*M*, it is expected that, all three proteins will be well retained, and none will elute in the induced gradient. However, depending on the displacer concentration, lysozyme may be displaced by the displacer or desorbed within the displacer front.

In Fig. 5, some example simulations over this range of displacement conditions are presented. In Fig. 5a, a relatively low displacer concentration of 5 m*M* neomycin sulfate is employed to displace a feed injection of 2 dimensionless time units. The first two components are well displaced by the neomycin sulfate. The third component, lysozyme, is desorbed within the displacer front, an example of the phenomena known as "selective displacement" [37]. In selective displacement, the significantly more and less strongly retained impurities are desorbed or eluted. Only the product and closely related impurities are displaced.

The presence of the lysozyme band within the displacer front hastens the breakthrough of the displacer front. Without lysozyme's presence, the neomycin sulfate front would be expected to break through at 11.5 dimensionless time units or about 0.5 dimensionless time units after the actual displacer breakthrough in Fig. 5a.

In Fig. 5b, the feed injection is increased to 6 dimensionless time units without changing the displacer concentration. In this simulation, a good separation is achieved between the product and the low and high affinity impurities; however, some nondevelopment has become evident. The more substantial mixed zone between the first band (artificial component 1) and the second band (cytochrome *c*) is an indication that the feed load is too large to be completely resolved by this length of column. Fur-

ther increasing the feed load will lead to serious nondevelopment and loss of yield.

In Fig. 5c, a higher displacer concentration of 30 m*M* neomycin sulfate is employed to displace a feed injection of 2 dimensionless time units. With this higher displacer concentration, the lysozyme is now effectively displaced by the neomycin sulfate leading to a three band isotactic profile, as expected based on the operating regime plot in Fig. 4. When the feed volume is increased to 4 dimensionless time units in Fig. 5d, nondevelopment is evident from the spike in protein concentration of the first band and from the increase in band overlap of the first two bands.

Comparing Fig. 5c and Fig. 5d it can be seen that nondevelopment becomes evident in two ways, through loss of the square band isotachic profile and through an increase in the degree of band overlap. The latter phenomena is particularly important in as much as it implies significant loss of product yield for injection sizes larger than that depicted in Fig. 5d when a displacer concentration of 30 m*M* neomycin sulfate is employed.

In Fig. 6a and Fig. 6b, production rate and yield are plotted versus feed time for the first separation problem. Four lines are given in each plot representing four different displacer concentrations. Arrows indicate the points corresponding to the separations presented in Fig. 5. It can be seen that, as the feed injection is increased by a factor of three from Fig. 5a to Fig. 5b, the production rate increases substantially (not quite tripling because the cycle time grows with the large feed injection). A similar increase in production rate can be seen from Fig. 5c to Fig. 5d. However, as the injection size is increased beyond those shown in Fig. 5b and Fig. 5d, the production rate falls due to loss of yield resulting from nondevelopment. In fact all of the curves in Fig. 6a and Fig. 6b share two properties. First, as the injection volume is increased, production rate increases while yield remains high. Second, as the injection volume is further increased, production rate and yield begins to fall after a certain point due to nondevelopment.

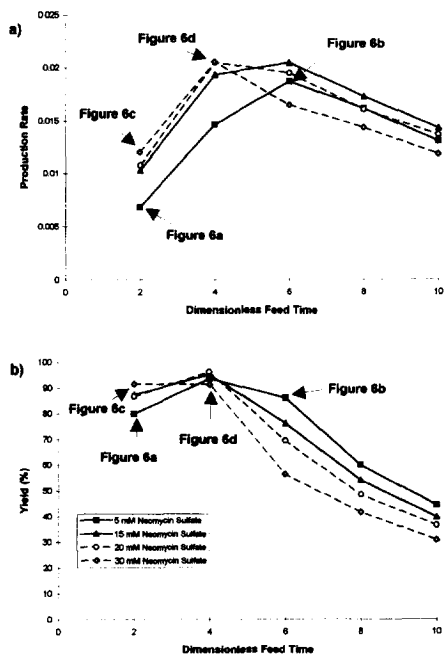

Fig. 6. Production rate and yield for displacement of feed stream 1. Displacement of 0.2 m*M* artificial component 1, 0.2 m*M* cytochrome *c* and 0.2 m*M* lysozyme by neomycin sulfate in 50 m*M* sodium ion concentration carrier. (a) Production rate versus dimensionless feed time for a range of displacer concentrations. (b) Yield rate versus dimensionless feed time for a range of displacer concentrations.

4.3. Separation problem 2 by displacement

The second model displacement problem was a separation of cytochrome *c* (the product) from a less retained impurity (artificial component 2) and a more strongly retained impurity (artificial component 3). Fig. 7 presents an operating regime plot for this problem. Both cytochrome *c* and artificial component 3 have similar elution and displacement properties. In a carrier with sodium ion concentration of 50 m*M*, these two components should be displaced over the range of displacer concentration from slightly less than 2 m*M* to greater than 40 m*M* neomycin sulfate. However, artificial component 2 has significantly less affinity for the stationary phase. As a result, it may elute by the induced salt gradient when the displacer concentration is greater than 30 m*M*.

In Fig. 8, some example simulations over this range of displacement conditions are presented. In Fig. 8a, a relatively low displacer concentration of 5 m*M* neomycin sulfate is employed to displace a feed

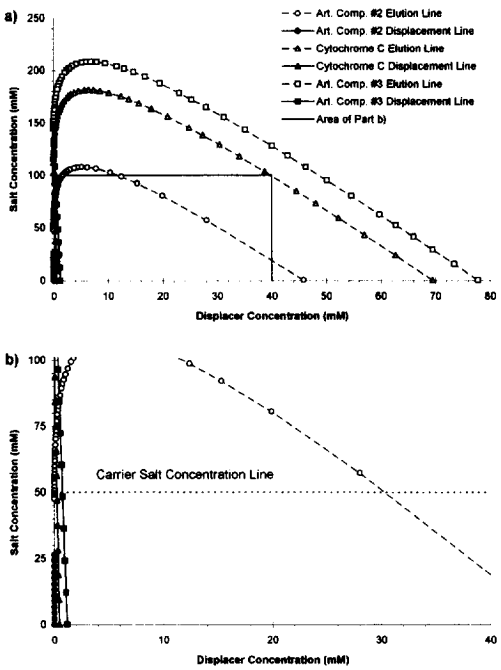

Fig. 7. Operating regime plot of feed stream 2. Elution and displacement lines of artificial component 3 (squares), cytochrome *c* (triangles) and artificial component 2 (circles) displaced by neomycin sulfate on strong cation exchanger. (a) Expanded view. (b) Close-up view.

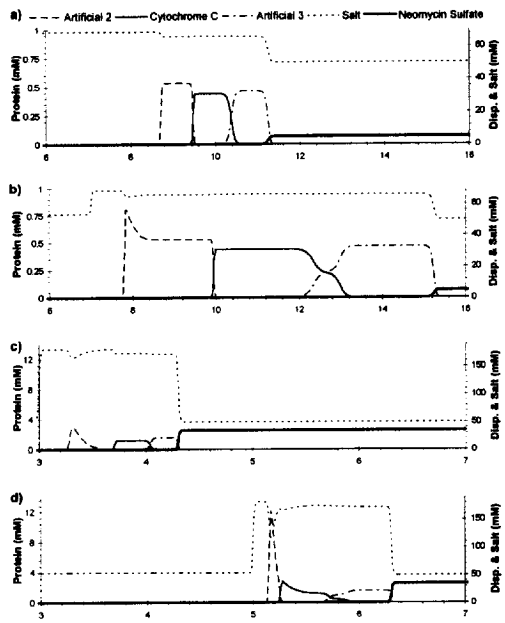

Fig. 8. Simulated displacement separations of feed stream 2. Displacement of 0.2 m*M* artificial component 2, 0.2 m*M* cytochrome *c* and 0.2 m*M* artificial component 3 by neomycin sulfate in 50 m*M* sodium ion concentration carrier. (a) 2.0 dimensionless time unit feed; 5 m*M* neomycin sulfate. (b) 6.0 dimensionless time unit feed; 5 m*M* neomycin sulfate. (c) 2.0 dimensionless time unit feed; 35 m*M* neomycin sulfate. (d) 4.0 dimensionless time unit feed; 35 m*M* neomycin sulfate.

injection of 2 dimensionless time units. All three components are displaced and form an isotactic square-wave train. Increasing the injection size to 6 dimensionless time units in Fig. 8b, leads to a small amount of nondevelopment with a mixed zone between the cytochrome *c* and the third component in the separation. Further increasing the feed load will lead to serious nondevelopment and loss of yield.

In Fig. 8c, a higher displacer concentration of 35 m*M* neomycin sulfate is employed to displace a feed injection of 2 dimensionless time units. As seen in the figure, the first component (artificial component) elutes in the induced salt gradient. An increase in the injection size to 4 dimensionless time units in Fig. 8d leads to nondevelopment. Further, the band of artificial component 2 appears not to elute in the induced gradient. In fact, it is eluting; however, the velocity at which cytochrome *c* band expands to its isotactic width is fast enough to catch up with the eluting band of artificial component 2.

In Fig. 9a and Fig. 9b, production rate and yield are plotted versus feed time for a number of different displacer concentrations. Arrows indicate the conditions corresponding to the separations presented in Fig. 8. As the feed injection size is increased by a factor of three from Fig. 8a to Fig. 8b, the productivity increases but fails to even double. This failure to increase at the same rate as the injection volume is due both to loss of yield and to the greater time required for loading of the feed. The greater increase in productivity from Fig. 8c to Fig. 8d can be attributed to a shorter cycle time and to a proportionally smaller loss in yield. In general, the same trends in productivity and yield apply to Fig. 9 as were previously observed in connection with Fig. 6. The major contrast between the two figures occurs

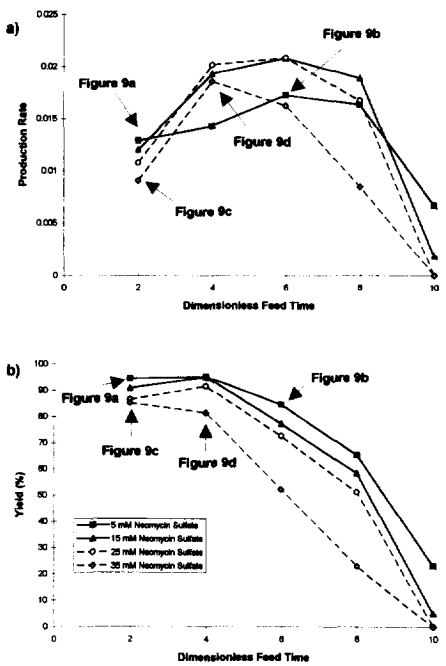

Fig. 9. Production rate and yield for displacement of feed stream 2. Displacement of 0.2 mM artificial component 2, 0.2 mM cytochrome c, and 0.2 mM artificial component 3 by neomycin sulfate in 50 mM sodium ion concentration carrier. (a) Production rate versus dimensionless feed time for a range of displacer concentrations. (b) Yield rate versus dimensionless feed time for a range of displacer concentrations.

at highest feed injection sizes. The productivity and yield drop off more precipitously for the second separation problem than they did for the first in the region of extreme nondevelopment (8 and 10 dimensionless time units).

5. Conclusions

In choosing the operating conditions of displacement chromatography, a number of issues come into play. If the choice of operating conditions were made solely on the basis of production rate, choice of displacer concentration and feed volume might be difficult since a number of different combinations of displacer concentration and feed volume often achieve similar productivity (see Fig. 6 and Fig. 9). However, from a practical viewpoint, use of a low concentration of displacer, which is nevertheless capable of displacing the product, may have significant advantages since low displaced concentration leads to a wide product zone. Because fraction collection will lead to some losses at both ends of the product zone, it may be desirable to have the widest possible zones. For example, the product zone in Fig. 5b is more than 2 dimensionless time units wide while the product zone in Fig. 5d is less than 1 dimensionless time unit wide.

In general, it is to be expected that proteins which are difficult to separate (i.e. groups of proteins which have small separation factors) will have similar operating regimes. Thus, it should be expected that two or more closely related proteins will form an isotactic displacement train in any optimized displacement separation. However, other components of the feed stream may be expected to elute from the column or be desorbed within the displacer front since biological feed streams possess components characterized by a broad range of chromatographic affinities. Thus, when selective displacement is conducted, a few closely related feed components will commonly form an isotactic displacement train while the bulk of the high affinity and low affinity impurities are desorbed or eluted.

6. Notation

C_i	mobile phase concentration (mM)
$C_{i,f}$	feed concentration (mM)
D_i	effective dispersion coefficient (cm^2/s)
F_i	function which returns Q_i when given $C_1, \ldots, C_{NC}$ (mM)
H	height equivalent to a theoretical plate (cm)
K_{1i}	equilibrium constant
k'	infinite dilution capacity factor [$\kappa' = (t_R - t_0)/t_0$)]
L	column length (cm)
N	number of theoretical plates
NC	number of components present in mobile phase
PR_i	production rate [μmol/(ml h)]
$\bar{Q}_i$	stationary phase concentration (mM)
Q_1	bound salt which is not sterically shielded (mM)

$\hat{Q}_{1i}$ bound salt which is sterically shielded by component i (mM)
t time (s)
t_{cyc} cycle time of a single chromatographic operation including regeneration
t_R retention time (s)
t_0 column dead time (s)
U velocity (cm/s)
u nondimensional velocity $u=U/u_0$
u_0 chromatographic velocity, $u_0=u_s/\epsilon$ (cm/s)
V_B breakthrough volume of a front (ml)
V_{col} empty column volume (ml)
V_f feed volume (ml)
V_{sp} stationary phase volume ($V_{sp}=(1-\epsilon)V_{col}$) (ml)
V_0 column dead volume ($V_0=\epsilon V_{col}$) (ml)
X axial position in column (cm)
x dimensionless axial position (X/L)
Y_i yield

6.1. Greek letters

α_{ij} separation factor
β phase ratio $\beta=[(1-\epsilon)/\epsilon]$
ϵ total porosity of column
Λ column capacity for a monovalent salt counterion (mM)
ν_i characteristic charge
σ_i steric factor
τ dimensionless time or column dead volumes ($\tau=t/t_0=V/V_0$)
τ_f dimensionless feed pulse time
τ_{sep} nondimensional time from end of injection until product finishes eluting

6.2. Subscripts

i mobile/stationary phase component number ($i=1$ designates salt)

Acknowledgments

This research was funded by Pharmacia Biotech and Grant CTS-9416921 from the National Science Foundation.

References

[1] J. Frenz and Cs. Horváth, in Cs. Horváth (Editor), High-Performance Liquid Chromatography, Academic Press, New York, 1988.
[2] S.M. Cramer and G. Subramanian, Sep. Purif. Methods, 19 (1990) 31.
[3] S.M. Cramer and G. Jayaraman, Current Opinion Biotechnol., 4 (1993) 217.
[4] F. Helfferich and D.B. James, J. Chromatogr., 46 (1970) 1.
[5] F. Helfferich and G. Klein, Multicomponent Chromatography, Marcel Dekker, New York, 1970.
[6] H. Rhee, R. Aris and N.R. Amundson, Trans. Royal Soc. London, 267 (1970) 419.
[7] H. Rhee and N.R. Amundson, AIChE J., 28 (1982) 423.
[8] J. Frenz and C. Horváth, AIChE J., 31 (1985) 400.
[9] R.W. Geldart, Q. Yu, P.C. Wankat and N.H.L. Wang, Sep. Sci. Technol., 21 (1986) 873.
[10] A.M. Katti and G. Guiochon, J. Chromatogr., 449 (1988) 25.
[11] M.W. Phillips, G. Subramanian and S.M. Cramer, J. Chromatogr., 454 (1988) 1.
[12] S. Golshan-Shirazi, M.Z. El Fallah and G. Guiochon, J. Chromatogr., 541 (1991) 195.
[13] Q. Yu and D.D. Do, J. Chromatogr., 538 (1991) 285.
[14] S.C.D. Jen and N.G. Pinto, J. Chromatogr., 590 (1992) 3.
[15] S.C.D. Jen and N.G. Pinto, React. Polym., 19 (1993) 145.
[16] T. Gu, Y. Truei, G. Tsai and G. Tsao, Chem. Eng. Sci., 47 (1992) 253.
[17] A. Felinger and G. Guiochon, Biotechnol. Bioeng., 41 (1993) 134.
[18] R.R. Drager and F.E. Regnier, J. Chromatogr., 359 (1986) 147.
[19] A. Velayudhan and C. Horváth, J. Chromatogr., 443 (1988) 13.
[20] R.D. Whitley, R. Wachter, F. Liu and N.H.L. Wang, J. Chromatogr., 465 (1989) 137.
[21] A. Velayudhan, Studies in Nonlinear Chromatography, Doctoral Dissertation, Yale University, New Haven, 1990.
[22] F.D. Antia and Cs. Horváth, J. Chromatogr., 556 (1991) 119.
[23] C.A. Brooks and S.M. Cramer, AIChE J., 38 (1992) 1969.
[24] P.K. de Bokx, P.C. Baarslag and H.P. Urbach, J. Chromatogr., 594 (1992) 9.
[25] J.C. Bellot and J.S. Condoret, J. Chromatogr. A, 657 (1993) 305.
[26] Y. Li and N. Pinto, J. Chromatogr. A, 702 (1994) 113.
[27] S.R. Gallant, A. Kundu and S.M. Cramer, J. Chromatogr. A, 702 (1995) 125.
[28] C.A. Brooks and S.M. Cramer, J. Chromatogr. A, 693 (1995) 187.
[29] C.A. Brooks and S.M. Cramer, Chem. Eng. Sci., (1996) in press.
[30] J.A. Gerstner and S.M. Cramer, Biotechnol. Progr., 8 (1992) 540.
[31] J.A. Gerstner and S.M. Cramer, BioPharm, 5 (1992) 42.
[32] G. Jayaraman, S.D. Gadam and S.M. Cramer, J. Chromatogr., 630 (1993) 53.

[33] G. Jayaraman, Y. Li, J.A. Moore and S.M. Cramer, J. Chromatogr. A, 702 (1995) 143.
[34] S.D. Gadam, S.R. Gallant and S.M. Cramer, AIChE J., 41 (1995) 1676.
[35] A. Kundu, S. Vunnum, G. Jayaraman, and S.M. Cramer, Biotechnol. Bioeng., 48 (1995) 452.
[36] A. Kundu, S. Vunnum and S.M. Cramer, J. Chromatogr. A, 707 (1995) 57.
[37] A. Kundu, S. Vunnum, S.M. Cramer, A. Kundu and S.M. Cramer, Selective Displacement Chromatography of Proteins, submitted to Biotech. Bioeng..
[38] S.R. Gallant, A. Kundu and S.M. Cramer, Biotechnol. Bioeng., 47 (1995) 355.
[39] S.R. Gallant, S. Vunnum and S.M. Cramer, J. Chromatogr. A, 725 (1996) 295.
[40] M.D. LeVan and T. Vermeulen, J. Phys. Chem., 85 (1981) 3247.
[41] A. Felinger and G. Guiochon, AIChE J., 40 (1994) 594.
[42] M. Czok and G. Guiochon, Anal. Chem., 62 (1990) 189.
[43] Z. Ma and G. Guiochon, Comput. Chem. Eng., 15 (1991) 415.
[44] S.D. Gadam, G. Jayaraman and S.M. Cramer, J. Chromatogr., 630 (1993) 37.